Atomistic Modeling and Simulation for Solving Gas Extraction Problems

Genri E. Norman, Vasily V. Pisarev, Grigory S. Smirnov and Vladimir V. Stegailov

Abstract Proof-of-concept results are presented on the application of molecular modeling and simulation to the gas extraction problems. Both hydrocarbon mixtures and gas hydrates in porous media are considered. Retrograde gas condensation reduces the amount of recoverable gas in reservoirs and can lead to jamming of wells. For example, the authors [1] developed a model of two-phase gas filtration through porous media that can reproduce the jamming. The model can describe gas flow in soil of reservoir if both a phase diagram of the gas mixture and permeability of pores to gaseous and liquid phases are known. Molecular dynamics simulations are used to study phase diagrams of binary hydrocarbon mixtures at temperatures between the critical points of pure components. The phase diagrams in free space and in slit pores are calculated. Effects of wall–gas interaction on the phase diagram are estimated. The data obtained from molecular simulations can be used to improve the hydrodynamic filtration model and to optimize the natural gas and gas condensate extraction conditions. Effects of pore structure on the phase stability of gas hydrates and on the diffusion of guest molecules are studied by means of molecular modeling. The anisotropic diffusion is found in hydrogen hydrates. Moreover, diffusivity of hydrogen molecules demonstrates anomalous behavior on nanosecond timescale.

Keywords Phase diagrams · Methane · Molecular dynamics · Clathrate hydrates · Retrograde condensation · Porosity

G.E. Norman · V.V. Pisarev (✉) · G.S. Smirnov · V.V. Stegailov
Joint Institute for High Temperatures of RAS, 125412 Moscow, Russia
e-mail: pisarevvv@gmail.com

G.S. Smirnov
Moscow Institute of Physics and Technology (State University),
141700 Dolgoprudnyy, Moscow Region, Russia

R.Q. Snurr et al. (eds.), *Foundations of Molecular Modeling and Simulation*,
Molecular Modeling and Simulation, DOI 10.1007/978-981-10-1128-3_9

1 Introduction

Natural gas extraction and storage give rise to a number of scientific and technical problems which require the knowledge of gas mixture behavior in porous media. Two particular problems are the modeling of hydrocarbon filtration through porous reservoir rocks and the modeling of gas–water systems at high pressures. They require the knowledge of phase diagrams and transport coefficients of multicomponent systems. Phase diagrams of one-component substances on the pressure (P)–temperature (T) plane consist of two-phase coexistence lines. Single-phase stability areas span between the lines. In contrast, a two-phase coexistence region transforms into a surface in the (P-T-α) space for binary mixtures phase diagrams, where α is the molar fraction of one of the components. In particular, there is a region of the two-phase surface for binary and multicomponent mixtures, where gas phase partially condenses into a liquid at the isothermal depressurizing. This phenomenon is known as retrograde condensation, and it can occur at temperatures higher than a critical temperature of the most volatile component of a mixture.

Since the critical temperature of methane is 190.6 K, methane-containing mixtures at ambient temperatures always have some range of methane concentrations at which the retrograde condensation occurs. This condensation complicates gas field operation, since it results in partial condensation of natural gas near a well bottom. It lowers a well yield and decreases the amount of recoverable hydrocarbons.

Gas filtration through a porous medium is often described mathematically in the form of the Darcy equation $u = KI$, where u is a filtration rate, I is a head gradient, and permeability coefficient K is the main characteristics of the medium. To model gas reservoirs, it is necessary to know permeability coefficients for both gas and liquid phases and to have a model to calculate reservoir liquid saturation [1, 2]. The equilibrium liquid saturation depends only on the thermodynamic functions of the fluids and reservoir walls.

The bulk phase diagrams of pure hydrocarbons and mixtures are well known from the experiments. In the work by Sage et al. [3], the bubble point pressures of methane + n-butane mixtures are determined experimentally from the discontinuity of isothermal compressibility of constant-composition mixture at the point of phase transition. The composition of vapor phase is determined in that work from the residual specific volume of gas. Later experiments employ phase recirculation techniques [4] to achieve vapor–liquid equilibrium [5, 6], and the phase compositions are analyzed by more advanced methods such as gas chromatography.

Molecule–wall interaction may shift phase diagrams in porous media, especially in nanopores. One of the ways to quantify such changes is the calculation of phase diagrams via atomistic simulations using molecular dynamics (MD) [7, 8] or Monte Carlo (MC) [9–13] methods. Semigrand ensemble simulations [12] and Gibbs–Duhem integration [13] are the most used MC techniques to tackle with the problem of multicomponent mixture phase diagram calculation. The MC approach is good for purely thermodynamic properties, but it does not allow calculation of dynamic properties. MD method is widely used for the calculation of phase diagrams [14],

structure [15–18], and transport properties [19, 20] of confined fluids. In the present work, we use the MD method for phase diagram calculations to validate the potential model. We plan to use the same potential model then in the future works to calculate the transport properties.

The phase diagram of a model methane + n-butane hydrocarbon mixture is studied in this paper. Such components are chosen because this mixture reproduces qualitatively phase diagram peculiarities of more complex hydrocarbons with the retrograde condensation, on one hand, and is studied experimentally at the Plast setup [1, 2] in the Joint Institute for High Temperatures of RAS, on the other hand. Due to the large critical temperature difference (190.6 K for methane vs. 425.1 K for butane), vapors below the critical point of methane have vanishing butane concentrations. Because of that, molecular simulations of phase equilibrium would require impractically large number of particles. For the gas extraction tasks, the supercritical region with respect to methane poses the greatest interest.

Modeling of natural gas with high water content poses an additional problem of gas hydrate formation. Clathrate gas hydrates are crystalline water-based inclusion compounds physically resembling ice. They require elevated pressures and low temperatures to be formed and are found in gas pipelines, permafrost regions, ocean sediments, comets, and certain outer planets [21, 22]. Guest molecules are trapped inside cavities, or cages, of the hydrogen-bonded water framework. The clathrate structure type is mainly determined by the size of guest molecules. Gas hydrates allow compact storage of hydrocarbons since one volume of hydrate may contain 180 volumes of gas (STP). The discovery of hydrogen hydrates (HH) attracted significant attention to the H_2 + H_2O phase diagram and clathrate structures. Along with the fundamental interest and significance for geophysics of icy moons and outer planets, HH provide a way to prospective hydrogen storage technologies. Diffusion of guest molecules plays a key role at hydrate storage and transportation. It affects the saturation of crystals with surrounding gases as well as the kinetics of clathrate decay and formation.

The diffusivity of hydrogen molecules is mostly studied for hexagonal ice and sII clathrate structure. Strauss [23] showed by neutron inelastic scattering that the diffusion coefficient of H_2 in deuterated ice at 25–60 K is rather high and comparable with the self-diffusion coefficient in liquid hydrogen. About 272 K, hydrogen solubility in hexagonal ice is comparable with that in liquid water at atmospheric pressure and differs by two times at 100 MPa [24].

In the clathrate structure sII, the diffusion coefficient of hydrogen molecules is lower by several orders of magnitude. The modeling of process of hydrogen molecule diffusion is performed previously in works [25–29]. Gorman et al. [28] reveal two diffusion modes in the sII structure: diffusion within one cavity on short timescale and “jumps” between cavities on long timescale.

The importance of hydrates requires the accurate knowledge of their thermodynamic and kinetic properties, mechanisms of formation and decay. Molecular simulation is a method of choice for such theoretical studies since it can explicitly capture the structure of gas hydrates and their constituents. MD is used to study different processes in methane hydrate, especially phase diagram of hydrates. Tung

et al. [30] determined the coexistence line in a wide range of pressures using TIP4P/Ew water model and OPLS-AA model for methane. They analyzed the evolution of the potential energy as a function of time during NPT simulations. Conde and Vega [31] used a similar technique to determine the coexistence points at up to 400 bar. They established that the TIP4P/Ice model [32] gives the best agreement with the experimental results, but their results differ from the Monte Carlo data of Jensen et al. [33]. In our previous work [34], we confirm the data of Jensen et al. [33] and suggest that TIP4P/2005 [35] water model gives better results at higher pressures than TIP4P/Ice.

Section 2 is devoted to the simulation details used at modeling of both problems. Simulation results are presented in Sect. 3. Phase diagrams for both bulk and porous systems are treated for gas condensates in Sects. 3.1 and 3.2. Melting and decay of the superheated sI methane hydrate structure are studied using MD simulation in Sect. 3.3. The melting curve is calculated by the direct coexistence simulations in a wide range of pressures up to 5 kbar for the SPC/E, TIP4P/2005, and TIP4P/Ice water models and the united atom model for methane. We also discuss diffusion of guest molecules in hydrogen hydrates in Sect. 3.4.

2 Simulation Details

2.1 Methane + n-Butane Mixture

TraPPE-UA (Transferrable Potential for Phase Equilibria–United Atom model) force field [36] is used for methane + n-butane mixtures. Methane molecules are presented by point particles, and butane molecules are reduced to four-particle models. Due to complications with rigid bonds in the MD method, a fully flexible butane molecule model is used instead of rigid bonds suggested in the original TraPPE force field. Spring constants for C–C bonds are taken from the AMBER force field [37]. Force field authors claim that phase diagrams are determined mainly by the intermolecular forces so such augmentation would still give the correct phase equilibrium [38]. Lennard-Jones (LJ) potential is used for nonbonded interactions. The LJ cutoff radius is 16 Å, and the potential and its derivative are smoothed to zero from 16 to 18 Å.

rRESPA scheme [39] is used for the numerical integration of motion equations. 4 fs timestep is chosen for nonbonded interactions, 2 fs for dihedral torsions, and 1 fs for bond and angle oscillations. Periodic boundary conditions are employed. The MD box size is chosen as $15 \times 15 \times N\, a_0^3$, where $a_0 = 6.8$ Å is the parameter of a simple cubic lattice and $N = 80$–250 depends on the target pressure and fraction of methane.

A following approach is applied to create a two-phase gas–liquid system. First, 9000 butane molecules are placed in the simple cubic lattice sites of the volume $15 \times 15 \times 40\, a_0^3$. The z-axis is a preferential direction in this configuration, which

is normal to the interface. The whole box volume is filled then with randomly distributed methane molecules. Energy minimization is then applied to relax the structure and move apart the particles which are generated unphysically close to each other. The number of methane molecules defines the mixture composition. Mixtures with 25–70 molar percentage of methane are considered.

Nose–Hoover thermostat [40] and Shinoda barostat [41] are applied at MD runs. As a fluid medium is simulated, the external pressure is established by changing only the L_z size of the simulation box to fit the P_{zz} pressure tensor component to the target value. The sizes L_x and L_y remain the same during the simulation, and the isotropic stress tensor is maintained hydrostatically by the fluid phases. The simulations are carried out for 1.5 million timesteps, or 6 ns, and component densities are then averaged over the last 500,000 timesteps in 100 bins along the z-axis to obtain the profiles.

2.2 Gas Hydrates

Although even simplified potential models can capture some important features of water, we have to use state-of-the-art classical potentials for accurate overall description of the water phase diagram in the solid phase. We use the TIP4P/Ice [32] model that gives a very good description of the ice phase coexistence lines. We consider for comparison TIP4P/2005 [35] and a well-known SPC/E [42] model. SPC/E is a simple 3-site model with charges located on H and O sites. TIP4P models are the 4-site models with a negative massless charge located near the oxygen atom and positive charges located on H atoms. We use a simple LJ model for methane and three-site model with charges for hydrogen molecules. The cross-interaction between guest and host molecules is described by the Lorentz–Berthelot rules:

$$\varepsilon_{ij} = \chi\sqrt{\varepsilon_{ii}\varepsilon_{jj}}, \sigma_{ij} = \left(\sigma_{ii} + \sigma_{jj}\right)/2, \quad (1)$$

where ε_{ii} and σ_{ii} are the LJ parameters for the pure ith component, and ε_{ij} and σ_{ij} are the cross-interaction parameters, where $\chi = 1$ or $\chi = 1.07$. The latter value indirectly introduces polarization of methane in TIP4P/2005 water [43].

We use 9 Å cutoff distance for the LJ interactions. The PPPM algorithm is applied to take into account the long-range interactions, with 9 Å cutoff for the real-space part. Water molecule bonds and angles are fixed using the SHAKE algorithm. The 3D periodic boundary conditions are used. The integration time step is 2 fs.

Diffusion of hydrogen molecules in hydrates is studied using the classical MD method. Our previous work shows the stability of C_0 and sT′ structures at pressures 2–10 atm. We study in the current work diffusion of hydrogen molecules at the pressure 0.6 GPa and temperatures from 140 to 260 K. The previous works show

that both structures are stable at those conditions at 100 % cage occupancy regardless of the potential used.

The simulations are performed with the Nose–Hoover thermostat and Shinoda barostat. The MSDs are calculated by both time averaging along the individual MD trajectories and ensemble averaging over several trajectories.

We determine first the equilibrium temperatures and pressures for coexistence. Conde and Vega in their work [31] performed similar calculations using long NPT MD trajectories (up to 1 μs). They waited for complete crystallization or complete melting of the initial three-phase system at several fixed temperatures. We follow another approach looking directly for the phase coexistence conditions.

We start from a $5 \times 5 \times 10$ unit cells clathrate system. Then, we keep atoms in one half of the cell frozen on their positions and raise the temperature in the other half to melt it. After such a procedure, we have the initial nonequilibrium system. Then, a short NPT simulation is performed to drive the system to the desired temperature and pressure. Finally, we perform a several nanosecond-long NVE MD simulation. The sI phase grows or melts in this simulation depending on whether we overshot or undershot the clathrate melting temperature at the given pressure. After partial melting or crystallizing, the system should stabilize at some temperature and pressure corresponding to the equilibrium curve. Reaching the equilibrium during crystallization requires longer simulation times, especially when methane molecules form a bubble in water. In our calculations, we consider only the cases when clathrate melts and equilibrium establishes much faster, during a few nanoseconds. When the volume of the sI phase stops changing, we assume that the temperature and pressure in the system correspond to the coexistence conditions.

All MD simulations are conducted using the LAMMPS package [44].

3 Simulation Results

3.1 Gas Condensates: Bulk Simulations

Density profiles of the hydrocarbon mixture components are calculated by MD simulations. The examples of the profiles are presented in Fig. 1 for temperature 330 K at two pressures. The liquid phase is butane-rich; the vapor phase is methane-rich. The density profiles turn out to be non-typical for a liquid film. Absolute value of the methane density does not change remarkably at the transition from vapor to liquid phase. Moreover, the absolute methane density is lower in liquid phase with respect to vapor at some conditions. It is interesting to note that there is a maximum of the methane density near the phase boundary at 40 atm. It points to the methane adsorption on the interface. Similar phenomena are observed at the modeling of the liquid in a contact with solid walls [15–17, 20], as well as in Coulomb clusters [45, 46].

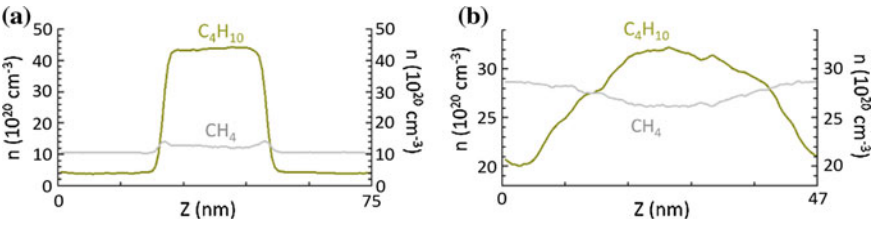

Fig. 1 Component density profiles in vapor–liquid coexistence simulations for methane + n-butane mixture at 330 K: 40 atm (**a**) and 90 atm (**b**)

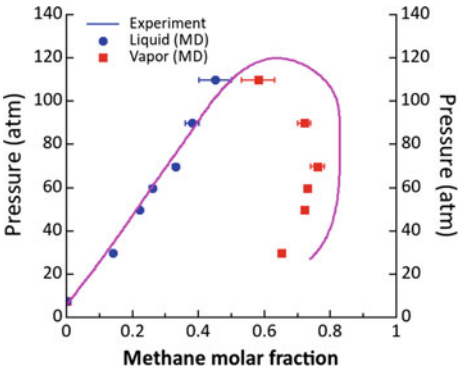

Fig. 2 Phase equilibrium curve of methane + n-butane at 330 K: MD model compared to the experimental data [3]. The error bars show statistical uncertainties. The error bars lie within the symbols if not shown

The phase equilibrium curve is calculated for the methane + n-butane mixture at 330 K (Fig. 2). The force field model used reproduces experimental data [3] on methane solubility in liquid butane rather well up to 80 atm. It reproduces the existence of the retrograde condensation region for the mixture under consideration at this temperature. The existence of the region follows from the fact that the phase equilibrium curve does not reach 100 % methane molar fraction.

3.2 *Gas Condensates: Pore Simulations*

Calculations are also performed for the phase equilibrium in a pore. The simplest model of a slit pore with smooth walls is considered. Interaction of a particle with walls is taken in the Lennard-Jones 9-3 form

$$U_{\text{wall}}(r) = \varepsilon_w \left[\frac{2}{15} \left(\frac{\sigma_w}{r} \right)^9 - \left(\frac{\sigma_w}{r} \right)^3 \right],$$

where r is a distance from a particle to the wall, and σ_w and ε_w are potential parameters. The walls are perpendicular to the x-axis. The examples of wall surfaces with ε_w = 0.35 kcal/mol, σ_w = 0.35 nm ("weak" wall potential) and ε_w = 0.5 kcal/mol, σ_w =

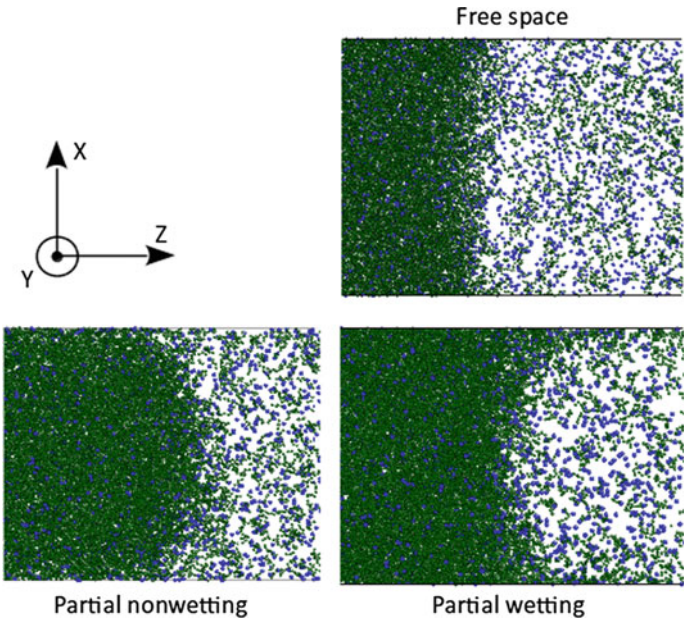

Fig. 3 Shape of the interphase boundary in the *XZ* plane for walls with different wettabilities at 330 K and 30 atm. Butane molecules are shown in *green* and methane molecules in *blue*. Every picture shows two overlaid snapshots of the simulation cell

0.39 nm ("strong" wall potential) are considered. The LJ parameters for the mixture components are ε_{CH4} = 0.29 kcal/mol and σ_{CH4} = 0.373 nm, ε_{CH3} = 0.19 kcal/mol and σ_{CH3} = 0.375 nm, and ε_{CH2} = 0.09 kcal/mol and σ_{CH2} = 0.395 nm. The simulations are conducted with the distances 4.08 and 10.2 nm between walls.

To obtain the density profiles in pores, we used longer simulations, for 2.5 million timesteps, or 10 ns. Density is averaged over the last 200,000 timesteps in 100 bins to obtain the profiles.

In the 10.2 nm pores, the different wettability of the walls is clearly seen. "Weak" walls show contact angle >90°, and "strong" walls show contact angle <90° (Fig. 3), which means partial wettability of the "strong" walls and partial nonwettability of "weak" walls. The mixture phase diagrams in the pores are shown in Fig. 4. The influence of the walls on the liquid phase composition is rather weak, while the shift of the vapor composition is more prominent. As expected, the effect is more for the stronger wall potential. In the case of "weak" wall, the shift of the vapor composition is within the statistical errors for 10.2 nm pore width, while the "strong" wall demonstrates effect on phase diagram for both pore widths.

An important result is the prominent shift of the mixture critical point with the 4.08 nm pore with "weak" potential. The critical pressure rises from around 120 atm in the bulk to about 140 atm in slit pore (Fig. 4). Since rocks usually have higher permeability to single-phase supercritical fluid than to two-phase mixture,

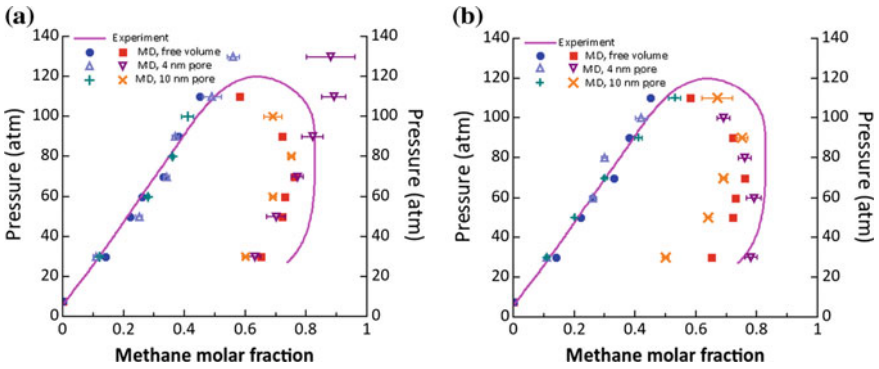

Fig. 4 Phase diagrams for methane + n-butane mixture at 330 K in slit pores with "weak" walls (**a**) and "strong" walls (**b**). *Triangles* 10.2 nm wide pores, crosses: 4.08 nm wide pores. *Circles*, *squares*, and *solid line* are the same as in Fig. 2. The error bars show statistical uncertainties. The error bars lie within the symbols if not shown

the widening of two-phase region may lead to lowering the permeability of nanoporous media.

As of yet, we cannot establish a clear relation between the phase composition shift and the pore width. In the case of the "strong" wall, the vapor composition shift relative to the bulk case has different signs depending on the pore width.

3.3 *Phase Diagram of Methane Hydrates*

Our results for different water models (TIP4P/Ice, TIP4P/2005, and SPC/E) are shown in Fig. 5.

According to Conde and Vega [31], the TIP4P/Ice model provides the best agreement with the experimental data. Jensen et al. [33] determined the sI melting line by free energy calculations via Monte Carlo method for TIP4P/Ice model, and the agreement of their results is worse than it was found by Conde and Vega (although the LJ potentials for methane were slightly different). Our MD results are in agreement with the data of Jensen et al. This is a strange fact because our results for TIP4P/2005 models are in a fairly good agreement with Conde and Vega. We attribute this discrepancy to the larger interface area of our model (5 × 5 unit cells compared to 2 × 2 in Conde and Vega's work). Presumably, smaller interface cross sections can result in larger statistical uncertainty and biased coexisting pressure and temperature values. Our results show that the TIP4P/2005 model gives the better agreement with the experimental coexistence line than the TIP4P/Ice model in the entire pressure range considered. Although TIP4P/2005 coexistence temperatures are systematically 10–20 K lower, the qualitative curve shape reproduces the experimental data quite well.

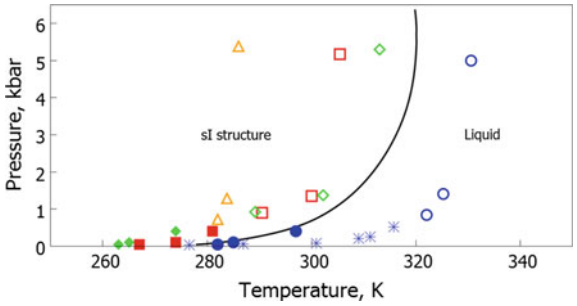

Fig. 5 Methane–water phase diagram. The *solid line* is the experimental [47] three-phase equilibrium curve of methane hydrate. The snowflakes show the result of Jensen et al. [33] for TIP4P/Ice model. The *filled blue*, *green*, and *red symbols* show the three-phase coexistence points of Conde and Vega [31], and *open symbols* show our results: *Yellow triangles* are for SPC/E, *green diamonds* and *red squares* for TIP4P/2005 with χ = 1:07 and 1.00 in (1), respectively, and *blue circles* for TIP4P/Ice. Our symbols correspond to 5510 unit cell systems. The statistical errors are within the symbols

3.4 Diffusion in Hydrogen Hydrates

We have studied in our previous work [48] the stability areas of the possible structures of the new phase at $\sim$0.5 GPa suggested by experimenters. It turns out that C_0 and *sT′* structures remain stable in the MD simulations.

We distinguish two characteristic time and length scales of diffusion in both C_0 and *sT′* structures. On the short timescale, hydrogen molecules move within a single cage (in *sT′* structure) or channel (in C_0 structure). On longer timescales, molecules jump between cages or channels. The jumps are rather rare events because molecules have to overcome high energy barriers.

Diffusion of guest molecules in C_0 and *sT′* structures shows prominent anisotropic and anomalous character, i.e., diffusion along different axes occurs at highly different rates, and the mean square displacement (MSD) does not grow linearly on time. Such behavior is probably due to the strong interaction between the framework and guest molecules, since the simulations of gases in metal–organic frameworks with large cage sizes do not reveal anomalous diffusion [49]

Water molecules in the C_0 structure form parallel helical channels oriented along the *z*-axis. Diffusion of hydrogen in the *XY* plane occurs therefore due to the jumps of molecules from one channel to another. The time- and ensemble-averaged MSDs of hydrogen molecules along each axis are shown in Fig. 6 in the double logarithmic scale. The asymptotical behavior of MSD curves at long timescales is shown for the lowest and highest of the studied temperatures. The MSD in the *z* direction (along the axis) is several orders higher than the MSD in the perpendicular plane. The MSDs in the *XY* plane do not exceed 0.1 nm^2 in 10 ns. This value is less than the square of the distance between channel centers. Therefore, most hydrogen molecules only move along the channel and do not jump between channels on this timescale.

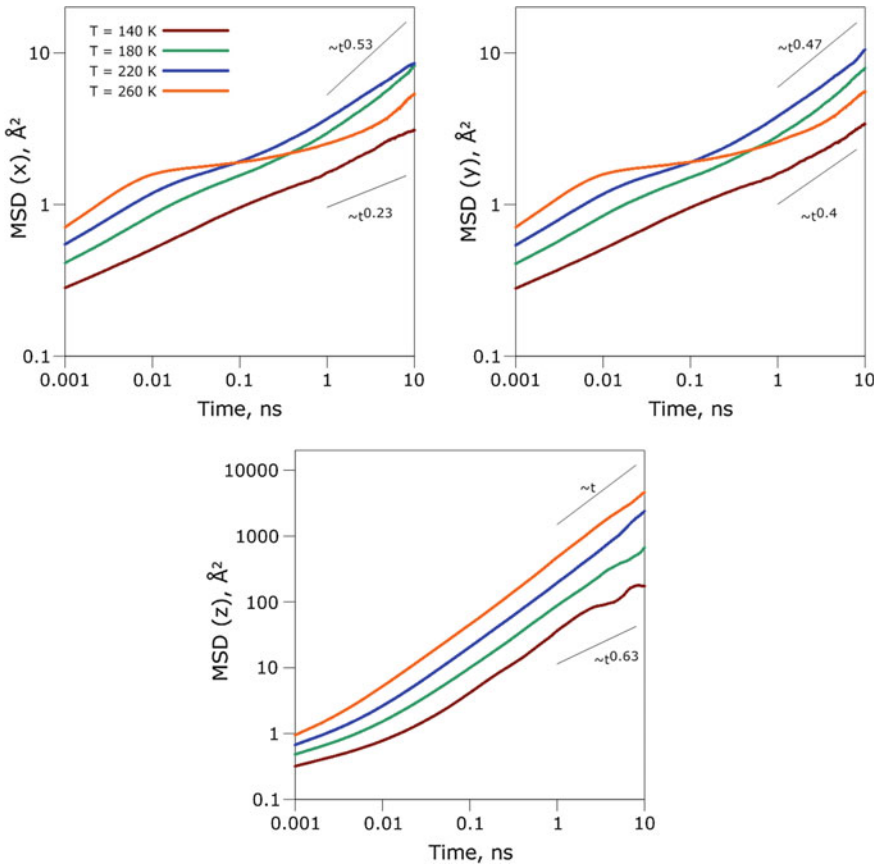

Fig. 6 Time- and ensemble-averaged mean square displacements of hydrogen molecules in the C_0 structure at different temperatures and 100 % cage occupancy

The MSDs along the *x*- and *y*-axes show peculiar behavior at 260 K. The high-temperature MSD curves cross the MSDs at 180 and 220 K. Thus, some inhibition of diffusion takes place at elevated temperatures. Its origin is yet unknown.

The diffusion of hydrogen molecules in the *sT′* structure is even slower (Fig. 7). The MSDs in 10 ns do not exceed 0.04 nm^2 along *x*- and *y*-axes and 0.006 nm^2 along the *z*-axis. The MSDs at 180 and 220 K reach the plateau corresponding to the trapping of molecules within a single polyhedron. Leaving a cage is a very improbable event, so the contribution of such jumps is negligible after ensemble averaging. At 140 K, the diffusion is so slow that only the *z* diffusion curve reaches the plateau. At 260 K, we see the growth of the MSD after a short plateau which corresponds to the jumps of hydrogen molecules between cages. The same behavior is expected for the lower temperatures at longer timescales.

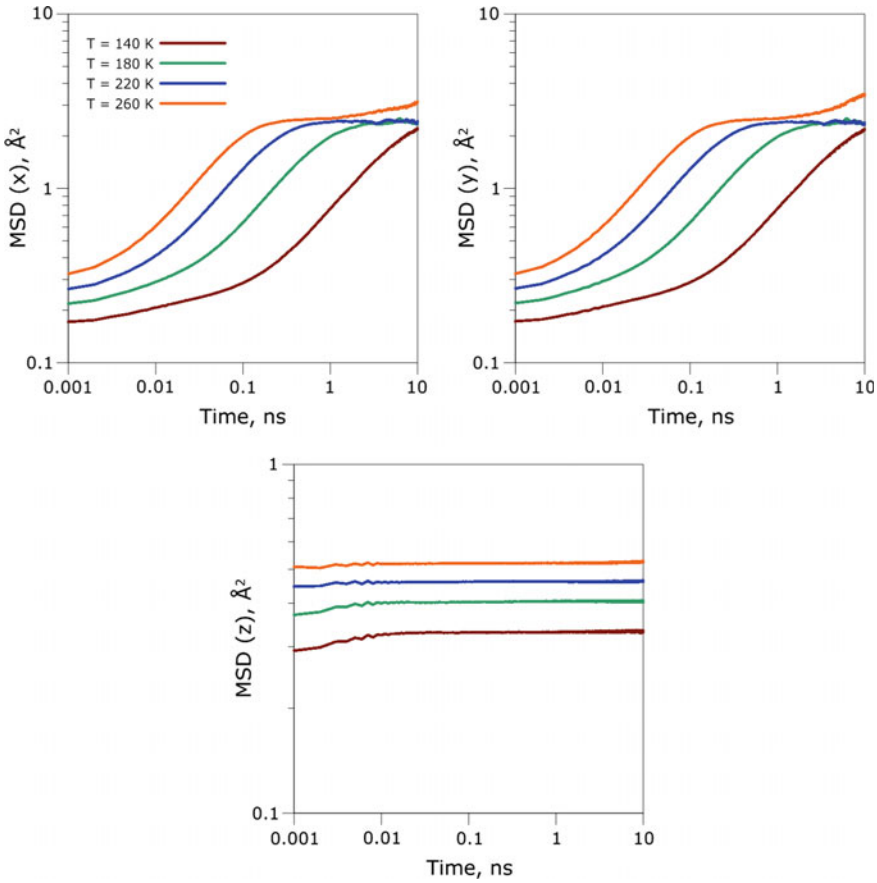

Fig. 7 Time- and ensemble-averaged mean square displacements of hydrogen molecules in the *sT'* structure at different temperatures and 100 % cage occupancy

The analysis of the displacements of the individual molecules shows that the MSDs in the *XY* plane are in fact due to large displacements of only a few molecules (several tens out of several hundred).

One of the important issues is the possibility to reveal the specific mechanisms of subdiffusion. The nonlinear time dependence of mean square displacements appears in different mathematical models, for example, in continuous-time random walk models, fractional Brownian motion, and diffusion on fractals. Sometimes, subdiffusion is a combination of different mechanisms. The more thorough investigation of subdiffusion mechanisms, subdiffusion–diffusion crossover times, diffusion coefficients, and activation energies is the subject of future works.

4 Summary

Two gas extraction problems are formulated to solve with the atomistic modeling. They are related to natural gas condensates and gas hydrates. First steps toward the multiscale modeling are suggested. Examples of molecular dynamics simulations are performed for phase diagrams and diffusion.

- The phase diagram of the test methane + n-butane system is calculated.
- The effect of nanoscale porosity on the test phase diagram is considered. Pore walls are shown to have more effect on the equilibrium vapor composition than on methane solubility. The effect of the critical point shift in nanopores is demonstrated.
- Three-phase coexistence lines are calculated for *sI* methane hydrate using different water models.
- Possible structures of hydrogen clathrate hydrates are refined at high pressures: C_0 and sT'.
- Anomalous diffusion of hydrogen molecules is analyzed in these structures, which is determined by the geometry features of the water framework. Diffusion of hydrogen molecules in the new C_0 and sT' hydrogen clathrate structures is also analyzed. Mean square displacement analysis shows that diffusion is anisotropic and anomalous at nanosecond timescale.

Acknowledgments The work is supported by the Russian Science Foundation grant 14-50-00124. The authors are thankful to prof. V.M. Zaichenko, who paid our attention to connection of our nucleation study with natural gas condensates modeling and to Drs V.V. Kachalov and V.M. Torchinskii for their interest to the work and valuable discussions.

References

1. Zaichenko, V.M., Maikov, I.L., Torchinskii, V.M., Shpil'rain, E.E.: Simulation of processes of filtration of hydrocarbons in a gas-condensate stratum. High Temp. **47**, 669-674 (2009)
2. Direktor, L.B., Zaichenko, V.M., Maikov, I.L., et al.: Theoretical and experimental studies of hydrodynamics and heat exchange in porous media. High Temp. **48**, 887–895 (2010)
3. Sage, B.H., Hicks, B.L., Lacey, W.N.: Phase equilibria in hydrocarbon systems. The methane-n-butane system in the two-phase region. Ind. Eng. Chem. **32**, 1085 (1940)
4. Muhlbauer, A.: Phase Equilibria: Measurement and Computation. CRC press (1997)
5. Kahre, L.C.: Low-temperature K data for methane-n-butane. J. Chem. Eng. Data **19**, 67–71 (1974)
6. Elliott, D.G., Chen, R.J.J., Chappelear, P.S., Kobayashi, R.: Vapor-liquid equilibrium of methane-n-butane system at low temperatures and high pressures. J. Chem. Eng. Data **19**, 71–77 (1974)
7. Norman, G.E., Stegailov, V.V.: Stochastic theory of the classical molecular dynamics method. Math. Models Comput. Simul. **5**, 305–333 (2013)
8. Rapaport, D.C.: The art of molecular dynamics simulation, 2nd edn. Cambridge University Press (2004)

9. Frenkel, D., Smit, B.: Understanding molecular simulation: from algorithms to applications. Academic Press (2002)
10. Norman, G.E., Filinov, V.S.: Investigation of phase transitions by a Monte-Carlo method. High Temp. **7**, 216–222 (1969)
11. Panagiotopoulos, A.Z.: Direct determination of phase coexistence properties of fluids by Monte Carlo simulations in a new ensemble. Mol. Phys. **61**, 813–826 (1987)
12. Kofke, D.A., Glandt, E.D.: Monte Carlo simulation of multicomponent equilibria in a semigrand canonical ensemble. Mol. Phys. **64**, 1105–1131 (1988)
13. Mehta, M., Kofke, D.A.: Coexistence diagrams of mixtures by molecular simulation. Chem. Eng. Sci. **49**, 2633–2645 (1994)
14. Kaneko, T., Mima, T., Yasuoka, K.: Phase diagram of Lennard-Jones fluid confined in slit pores. Chem. Phys. Lett. **490**, 165–171 (2010)
15. Fomin, YuD: Molecular dynamics simulation of benzene in graphite and amorphous carbon slit pores. J. Comput. Chem. (2013). doi:10.1002/jcc.23429
16. Fomin, YuD, Tsiok, E.D., Ryzhov, V.N.: The behavior of benzene confined in single wall carbon nanotube. J. Comput. Chem. (2015). doi:10.1002/jcc.23872
17. Fomin, YuD, Tsiok, E.D., Ryzhov, V.N.: The behavior of cyclohexane confined in slit carbon nanopore. J. Chem. Phys. **143**, 184702 (2015)
18. Rudyak, V.Ya., Belkin, A.A., Egorov, V.V., Ivanov, D.A.: About fluids structure in microchannels. Int. J. Multiphys. **5**, 145–155 (2011)
19. Rudyak, V.Ya., Belkin, A.A.: Fluid viscosity under confined conditions. Doklady Phys. **59**, 604–606 (2014)
20. Johnston, K., Harmandaris, V.: Properties of benzene confined between two Au(111) surfaces using a combined density functional theory and classical molecular dynamics approach. J. Phys. Chem. C **115**, 14707–14717 (2011)
21. Moustafa, S.G., Schulz, A.J., Kofke, D.A.: Effects of finite size and proton disorder on lattice-dynamics estimates of the free energy of clathrate hydrates. Ind. Eng. Chem. Res. **54**, 4487–4496 (2015)
22. Skripov, V.P., Faizullin, M.Z.: Crystal-Liquid-Gas Phase Transitions and Thermodynamic Similarity. Wiley-VCH, Berlin-Weinheim (2006)
23. Strauss, H.L., Chen, Z., Loong, C.-K.: The diffusion of H_2 in hexagonal ice at low temperatures. J. Chem. Phys. **101**, 7177 (1994)
24. Ildyakov, A.V., Manakov, A.Y.: Solubility of hydrogen in ice Ih at pressures up to 8 MPa. Int. J. Hydrogen Energy **39**, 18958–18961 (2014)
25. Alavi, S., Ripmeester, J.A.: Hydrogen-gas migration through clathrate hydrate cages. Angew. Chem. Int. Ed. Engl. **46**, 6102–6105 (2007)
26. Frankcombe, T.J., Kroes, G.-J.: Molecular dynamics simulations of type-sII hydrogen clathrate hydrate close to equilibrium conditions. J. Phys. Chem. C **111**, 13044 (2007)
27. Iwai, Y., Hirata, M.: Molecular dynamics simulation of diffusion of hydrogen in binary hydrogen–tetrahydrofuran hydrate. Mol. Simul. **38**, 333–340 (2012)
28. Gorman, P.D., English, N.J., MacElroy, J.M.D.: Dynamical cage behaviour and hydrogen migration in hydrogen and hydrogen-tetrahydrofuran clathrate hydrates. J. Chem. Phys. **136**, 044506 (2012)
29. Cao, H., English, N.J., MacElroy, J.M.D.: Diffusive hydrogen inter-cage migration in hydrogen and hydrogen-tetrahydrofuran clathrate hydrates. J. Chem. Phys. **138**, 094507 (2013)
30. Tung, Y.-T., Chen, L.-J., Chen, Y.-P., Lin, S.-T.: The growth of structure I methane hydrate from molecular dynamics simulations. J. Phys. Chem. B. **114**, 10804–10813 (2010)
31. Conde, M.M., Vega, C.: Determining the three-phase coexistence line in methane hydrates using computer simulations. J. Chem. Phys. **133**, 064507 (2010)
32. Abascal, J.L.F., Sanz, E., García Fernández, R., Vega, C.: A potential model for the study of ices and amorphous water: TIP4P/Ice. J. Chem. Phys. **122**, 234511 (2005)
33. Jensen, L., Thomsen, K., von Solms, N., et al.: Calculation of liquid water−hydrate−methane vapor phase equilibria from molecular simulations. J. Phys. Chem. B **114**, 5775–5782 (2010)

34. Smirnov, G.S., Stegailov, V.V.: Melting and superheating of sI methane hydrate: molecular dynamics study. J. Chem. Phys. **136**, 044523 (2012)
35. Abascal, J.L.F., Vega, C.: A general purpose model for the condensed phases of water: TIP4P/2005. J. Chem. Phys. **123**, 234505 (2005)
36. Martin, M.G., Siepmann, J.I.: Transferable potentials for phase equilibria. 1. united-atom description of n-alkanes. J. Phys. Chem. B **102**, 2569–2577 (1998)
37. Cornell, W.D., Cieplak, P., Bayly, C.I., et al.: A second generation force field for the simulation of proteins, nucleic acids, and organic molecules. J. Am. Chem. Soc. **117**, 5179–5197 (1995)
38. Chen, B., Siepmann, J.I.: Transferable potentials for phase equilibria. 3. explicit-hydrogen description of normal alkanes. J. Phys. Chem. B **103**, 5370–5379 (1999)
39. Tuckerman, M., Berne, B.J., Martyna, G.J.: Reversible multiple time scale molecular dynamics. J. Chem. Phys. **97**, 1990–2001 (1992)
40. Hoover, W.G.: Canonical dynamics: equilibrium phase-space distributions. Phys. Rev. A **31**, 1695 (1985)
41. Shinoda, W., Shiga, M., Mikami, M.: Rapid estimation of elastic constants by molecular dynamics simulation under constant stress. Phys. Rev. B **69**, 134103 (2004)
42. Berendsen, H.J.C., Grigera, J.R., Straatsma, T.P.: The missing term in effective pair potentials. J. Phys. Chem. **91**, 6269–6271 (1987)
43. Docherty, H., Galindo, A., Vega, C., Sanz, E.: A potential model for methane in water describing correctly the solubility of the gas and the properties of the methane hydrate. J. Chem. Phys. **125**, 074510 (2006)
44. Plimpton, S.J.: Fast parallel algorithms for short-range molecular dynamics. J. Comp Phys. **117**, 1–19 (1995)
45. Raitza, T., Reinholz, H., Röpke, G., et al.: Laser excited expanding small clusters: single time distribution functions. Contrib. Plasma Phys. **49**, 496–506 (2009)
46. Morozov, I.V., Kazennov, A.M., Bystryi, R.G., et al.: Molecular dynamics simulations of the relaxation processes in the condensed matter on GPUs. Comp. Phys. Comm. **182**, 1974–1978 (2011)
47. Dyadin, Y.A., Aladko, E.Y.: In: Monfort, J. (ed.) Proceedings of the Second International Conference on Natural Gas Hydrates, pp. 67–70 (1996)
48. Smirnov, G.S., Stegailov, V.V.: Toward determination of the new hydrogen hydrate clathrate structures. J. Phys. Chem. Lett. **4**, 3560–3564 (2013)
49. Borah, B., Zhang, H., Snurr, R.Q.: Diffusion of methane and other alkanes in metal-organic frameworks for natural gas storage. Chem. Eng. Sci. **124**, 135–143 (2015)